Proceedings of ASME Turbo Expo 2011
GT2011
June 6-10, 2011, Vancouver, British Columbia, Canada

GT2011-45209

MEASURED STATIC AND ROTORDYNAMIC COEFFICIENT RESULTS FOR A ROCKER-PIVOT, TILTING-PAD BEARING WITH 50 AND 60% OFFSETS

Chris D. Kulhanek
Graduate Research Assistant
chris.kulhanek@swri.org

Dara W. Childs
Leland T. Jordan Professor of Mechanical Engineering
dchilds@tamu.edu

Turbomachinery Laboratory
Texas A&M University
College Station, TX 77843-3123

ABSTRACT

Static and rotordynamic coefficients are measured for a rocker-pivot, tilting-pad journal bearing (TPJB) with 50 and 60% offset pads in a load-between-pad (LBP) configuration. The bearing uses leading-edge-groove direct lubrication and has the following characteristics: 5-pads, 101.6 mm (4.0 in) nominal diameter, .0814 - .0837 mm (.0032 - .0033 in) radial bearing clearance, .25 to .27 preload, and 60.325 mm (2.375 in) axial pad length. Tests were performed on a floating bearing test rig with unit loads from 0 to 3101 kPa (450 psi) and speeds from 7 to 16 krpm.

Dynamic tests were conducted over a range of frequencies (20 to 320 Hz) to obtain complex dynamic stiffness coefficients as functions of excitation frequency. For most test conditions, the real dynamic stiffness functions were well fitted with a quadratic function with respect to frequency. This curve fit allowed for the stiffness frequency dependency to be captured by including an added mass matrix [M] to a conventional [K][C] model, yielding a frequency independent [K][C][M] model. The imaginary dynamic stiffness coefficients increased linearly with frequency, producing frequency-independent direct damping coefficients. Direct stiffness coefficients were larger for the 60% offset bearing at light unit loads. At high loads, the 50% offset configuration had a larger stiffness in the loaded direction, while the unloaded direct stiffness was approximately the same for both pivot offsets. Cross-coupled stiffness coefficients were positive and significantly smaller than direct stiffness coefficients. Negative direct added-mass coefficients were obtained for both offsets, especially in the unloaded direction. Cross-coupled added-mass coefficients are generally positive and of the same sign. Direct damping coefficients were mostly independent of load and speed, showing no appreciable difference between pivot offsets. Cross-coupled damping coefficients had the same sign and were much smaller than direct coefficients.

Measured static eccentricities suggested cross-coupling stiffness exists for both pivot offsets, agreeing with dynamic measurements. Static stiffness measurements showed good agreement with the loaded, direct dynamic stiffness coefficients.

NOMENCLATURE

$\boldsymbol{A_{ij}}$	Fourier transforms for the measured stator acceleration. (e.g. acceleration in "*j*" direction due to a force in the "i" direction) [L/t^2]
C_{ij}	Damping coefficients [F.t/L]
C_b	Radial bearing clearance [L]
C_p	Radial pad clearance [L]
D	Bearing diameter [L]
$\boldsymbol{D_{ij}}$	Fourier transforms for the measured stator relative motion [L]
$\boldsymbol{F_{ij}}$	Fourier transforms for the measured stator force [F]
F_s	Static force applied by pneumatic loader [F]
f_{bx} f_{by}	Bearing reaction force component in the *x*,*y* direction respectively [F]
f_x f_y	Measured excitation force component in the *x*,*y* direction [F]
$\boldsymbol{H_{ij}}$	Dynamic stiffness coefficients [F/L]
$\boldsymbol{j}$	$\sqrt{-1}$
K_{ij}	Stiffness coefficients [F/L]
L	Pad length [L]
M_s	Mass of the stator [M]
M_{ij}	Added-mass coefficients [M]
$\ddot{x}_s$ $\ddot{y}_s$	Absolute stator acceleration [L/t^2]
Δx Δy	Relative rotor to stator motion [L]
ω	Running speed of rotor [1/t]
Ω	Excitation frequency of stator [1/t]

Abbreviations

FFT	Fast Fourier Transform
LBP	Load-between-pad
LOP	Load-on-pad
TPJB	Tilting-pad journal bearing

Subscripts

x,*y*	*x* (unloaded) and *y* (loaded) directions
i,*j*	*x*,*y*

INTRODUCTION

Tilting-pad journal bearings (TPJBs) are commonly used in rotating machines because of their substantial stability benefits over conventional, fixed-geometry journal bearings. TPJBs have multiple pads that rotate to balance fluid film forces, directing reaction forces to the rotor center and promoting stability. A rocker-pivot TPJB similar to the bearing tested is shown in Fig. 1.

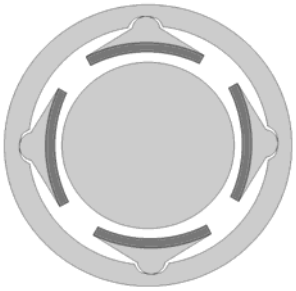

Fig. 1. Rocker-pivot tilting-pad journal bearing.

The fluid film forces acting between a TPJB and rotor can often be modeled as a linearized two degree-of-freedom system with stiffness and damping matrices, as shown in Eq. 1.

$$-\begin{Bmatrix} f_{bx} \\ f_{by} \end{Bmatrix} = \begin{bmatrix} K_{xx} & K_{xy} \\ K_{yx} & K_{yy} \end{bmatrix} \begin{Bmatrix} \Delta x \\ \Delta y \end{Bmatrix} + \begin{bmatrix} C_{xx} & C_{xy} \\ C_{yx} & C_{yy} \end{bmatrix} \begin{Bmatrix} \Delta \dot{x} \\ \Delta \dot{y} \end{Bmatrix} \quad (1)$$

In 1964, Lund [1] presented the original technique of summing the contribution of each pad to obtain combined stiffness and damping for two orthogonal directions that fits the model described in Eq. (1). Lund presented stiffness and damping design curves for multiple tilting pad bearing configurations. Eq.(1) includes rotordynamic coefficients that can depend on excitation frequency. Since Lund's work, many analyses have been conducted on TPJB rotordynamic coefficients of Eq.(1) suggesting that they are frequency dependent.

Experimental data concerning this possible frequency-dependency is more limited. Ha and Yang [2] reported one of the first studies in 1999. They tested a 5-pad, 300 mm (11.8 in) diameter TPJB in load-on-pad (LOP) configuration. Test conditions included speeds up to 3600 rpm and static unit loads of 111 and 222 kPa (16 and 32 psi). Dynamic testing involved single excitation frequencies, ranging from .5 to 2 times running speed. They reported that stiffness coefficients slightly decreased with increasing excitation frequency while damping coefficients slightly increased with excitation frequency. There excitation frequencies were limited to 60 Hz at relatively low speeds.

In 2001, Wygant [3] tested a five-pad, 70mm (2.76 in) diameter, rocker-pivot, TPJB. The bearing had an 81.3 μm (3.2 mil) clearance, L/D=.75, and 50 % offset pads. Testing was conducted at speeds to 2250 rpm and loads near 690 kPa (100 psi). While altering pad preload and pivot type, Wygant also examined the effect of excitation frequency on the dynamic coefficients. The bearing was excited with single frequency orbital excitations at .5, 1, and 2 times ω, producing frequency dependent stiffness and damping coefficients. Quantifying frequency dependency of the direct damping coefficients is difficult due to the limited excitation frequencies and uncertainties. The direct stiffness coefficients were found to decrease with increasing frequency, consistent with the results of Ha and Yang [2].

Recent investigations regarding frequency-dependency include the work of Rodriguez and Childs [4] who tested a four-pad, flexure-pivot, TP bearing with 50 % offset pads in a LOP configuration. The test bearing had 116.8 mm (4.6 in) nominal diameter, .19 mm (7.5 mil) C_b, and .25 preload. Test conditions included speeds from 6 to 16 krpm, and unit static loads to 1034 kPa (150 psi). Complex dynamic stiffness coefficients were obtained from multi-frequency excitation including frequencies from 20 to 300 Hz. The real dynamic stiffness coefficients were frequency dependent, and generally decreased with increasing frequency. The imaginary dynamic stiffness coefficients increased linearly with frequency, implying a constant, frequency-independent damping coefficient. By applying the [K][C][M] model shown below in Eq. (2), the frequency dependency of the stiffness was captured by an added-mass, or apparent mass matrix, [M].

$$-\begin{Bmatrix} f_{bx} \\ f_{by} \end{Bmatrix} = \begin{bmatrix} K_{xx} & K_{xy} \\ K_{yx} & K_{yy} \end{bmatrix} \begin{Bmatrix} \Delta x \\ \Delta y \end{Bmatrix} + \begin{bmatrix} C_{xx} & C_{xy} \\ C_{yx} & C_{yy} \end{bmatrix} \begin{Bmatrix} \Delta \dot{x} \\ \Delta \dot{y} \end{Bmatrix} + \begin{bmatrix} M_{xx} & M_{xy} \\ M_{yx} & M_{yy} \end{bmatrix} \begin{Bmatrix} \Delta \ddot{x} \\ \Delta \ddot{y} \end{Bmatrix} \quad (2)$$

Al-Ghasem and Childs [5], and Hensley and Childs [6] tested the same bearing at different loads in LBP configurations. They were also able to account for the observed coefficient frequency dependency by applying a [K][C][M] model.

In 2006, Dmochowski [7] performed an experimental and theoretical investigation of the dynamic coefficients of a rocker-pivot bearing. He tested a five-pad bearing with a 98 mm (3.858 in) diameter, .3 preload, and an unspecified offset. Tests were conducted at ω = 9 krpm with unit loads of 460 and 1160 kPa (67 and 168 psi). Two bearing configurations were considered, including an LBP case with L/D=0.4 and an LOP case with L/D=1. Dynamic testing included a multi-frequency excitation range up to 300 Hz. Although the measured dynamic results showed some scatter, the direct dynamic stiffness coefficients exhibited trends that could be fit with a [K][C][M] model.

Recently, Carter and Childs [8] tested a 5-pad rocker-pivot TP bearing in LBP and LOP configurations. The pads had a 60% pivot offset and were direct lubricated with leading-edge-groove (LEG) technology. The bearing had the same nominal dimensions as the bearing tested in this paper. Dynamic and static tests were performed at ω = 4 to 13 krpm with unit static loads from 345 kPa to 3101 kPa (50 to 450 psi). A multi-frequency excitation was used to obtain complex dynamic stiffness coefficients. For the majority of the test conditions, the real part of the dynamic stiffnesses could be approximated as quadratic functions of excitation frequency. These trends agreed with Dmochowski's measured results [7], producing a frequency-independent [K][C][M] model. The direct damping terms showed no frequency dependency and changed very little with respect to speed and load.

Childs and Harris [9] provide dynamic measurements for a 101.6 mm (4 in) diameter, 4-pad, ball-in-socket, tilting-pad bearing. The test bearing had a 95.3μm (3.75 mil) radial bearing clearance and a mean loaded pad preload of .37. Using multi-frequency excitation, dynamic stiffness coefficients were obtained for speeds to 12 krpm and loads to 1896 kPa (275 psi). Rotordynamic coefficients were determined from curve fitting the complex dynamic stiffness coefficients with respect to frequency. The frequency-independent, [K][C][M] model produced average uncertainties for the direct stiffness, damping, and added-mass coefficients of 2, 10, and 25% respectively.

Carter and Childs' [8] results led some researchers to state that a rocker-pivot TPJB with a 50% pivot offset is more likely to exhibit frequency dependency. This belief is consistent with some predictions, e.g., Schmeid, et al. [10], who present a dynamic model for TPJBs that includes the pad inertias and pad rotational angles. Predictions for dynamic coefficients are made by solving the Reynolds Equation for the perturbed equilibrium position. Stiffness and damping coefficients are presented as functions of excitation frequency for three LBP bearing configurations that alter pad number and pivot offset. Simulations were for ω = 6000 rpm and a static load

of 500 kPa (73 psi). The four-pad bearing with 55% offset yields rotordynamic coefficients that are highly frequency-dependent, and cannot be modeled with (only) additional added-mass terms. The direct stiffness coefficients decrease while direct damping coefficients increase in sub-synchronous range. The coefficients of the five-pad bearing with 55% offset exhibit less frequency dependency. The four-pad bearing with 60% offset provides stiffness and damping coefficients that are frequency-independent.

Most recently, Delgado et al. [11] tested two rocker-pivot, tilting-pad bearing in several configurations. They tested a five-pad bearing with .16 preload in LOP configuration and a four-pad bearing with .3 preload in LBP configuration. Both bearings were tested with 50 and 60% pivot offsets. The test bearings were directly lubricated and had a nominal 110 mm (4.3 in) diameter. Testing was performed at 7.5, 10, and 15 krpm with a static unit load of 300 kPa (44 psi). Dynamic stiffness coefficients for the test bearings were obtained from multi-frequency excitation. The direct rotordynamic coefficients were identified from curve fitting. All measured results were adequately modeled by a frequency-independent [K][C][M] model.

The current work presents measured rotordynamic coefficients for 5-pad rocker-pivot tilting-pad bearing with 50 and 60% pivot offsets. The test bearing is almost identical to that tested by Childs and Carter [8], but includes 50% pivot offset pads. Additionally, Delgado et al. [11] tested a 5-pad bearing in LOP at light static loads while the results presented here are for a 5-pad bearing in LBP at significantly higher static loads. While this paper presents only experimental results, a full comparison with predictions is presented by Kulhanek [12].

TEST RIG DESCRIPTION

The test rig shown in Fig. 2 was designed by Kaul [13] and uses a floating test bearing design, similar to that used by Glienicke [14].

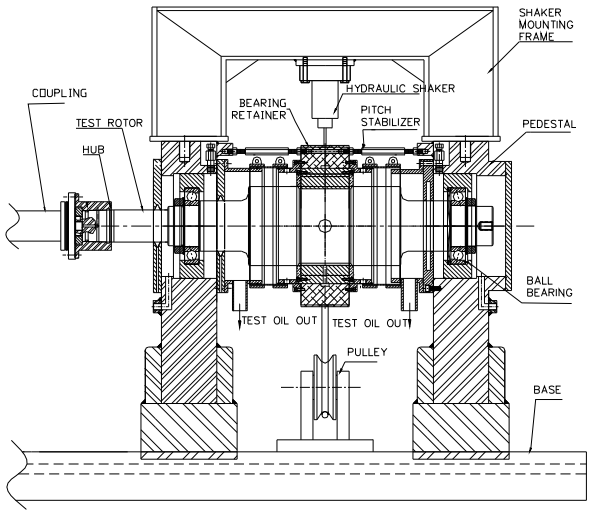

Fig. 2. Test rig main section [4].

The rig uses a 65 kW (87 HP) air turbine drive motor that can produce speeds up to 17 krpm. The rotor has a diameter of 101.59 mm (3.9995 in) at the test section and is supported on steel pedestals with mist lubricated, hybrid-ceramic, ball bearings. Angular alignment between the rotor and test bearing is provided by an arrangement of six pitch stabilizers. ISO VG32 turbine oil is the test lubricant.

Static and Dynamic Loading

The loading of the test bearing consists of two orthogonal dynamic forces and a one-directional static load. Hydraulic shakers provide dynamic loads in the *x* and *y* directions through stinger elements. A pneumatic loader applies static loads up to 22 kN (4900 lb) in the *y* direction only. A schematic of stator arrangement is shown in Fig. 3, as observed from the drive end of the test rig.

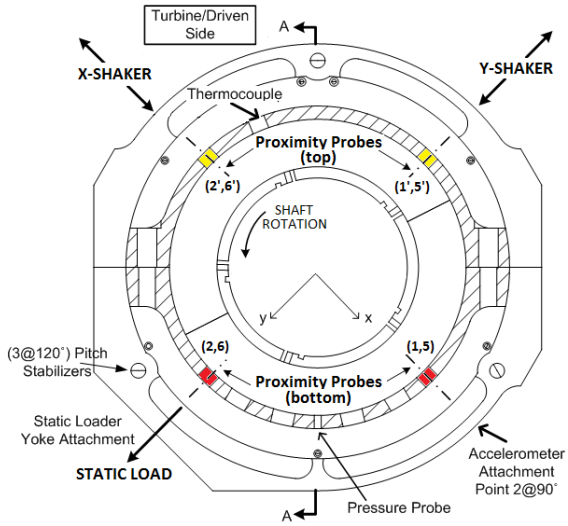

Fig. 3. Stator and test bearing viewed from the drive end.

Instrumentation

The stator section in Fig.(3) holds the test bearing and all associated instrumentation. Four proximity probes, located in the stator end caps, record the relative rotor-stator motion for each direction of excitation. These measurement in two parallel planes allows monitoring of the stator's pitch and provides an average bearing position. Piezoelectric accelerometers measure the stator absolute acceleration in both the *x* and *y* directions. Thermocouples are located in the oil-inlet chamber as well as the downstream end caps. Pressure probes measure the oil pressure at the inlet and both of the outlet locations. The oil flow-rate is measured with an up-stream turbine flow-meter.

Test Bearing

Figure 4 illustrates the 5-pad, rocker-pivot, titling-pad test bearing that uses the same split-design bearing shell as tested by Carter and Childs [8]. The bearing assembly includes two different pad sets to obtain pivot offsets of 50 and 60%. All pads are directly lubricated by a leading-edge groove, or LEG. A flooded configuration is used where floating end seals prevent axial leakage out of the bearing. This design requires the majority of the oil from each pad to exit through ports in the bearing shell. A total of 13 oil ports direct the oil to the non-drive end of the bearing housing.

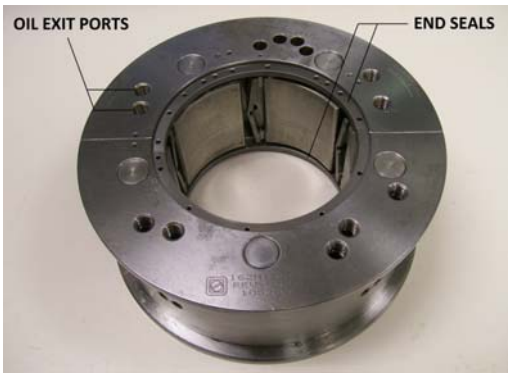

Fig. 4. Oil exit ports and end seals of test bearing.

A summary of the test bearing geometry, loading arrangement, and lubricant type are presented below in Table 1. The measured bearing clearances and preloads are given in Table 2. The bearing clearance was measured with the motion probes while the preload was calculated from the measured C_b and C_p.

Table 1. Test bearing parameters.

Number of Pads	5
Configuration	LBP
Pad Arc Angle, θ	57.87°
Rotor Diameter	101.587 mm (3.9995 in)
Pad Axial Length	60.325 mm (2.375 in)
Radial Pad Clearance, C_p	.112 mm (.0044 in)
Pad Mass	.44 kg (.96 lbm)
Lubricant Type	ISO VG 32

Table 2. Test bearing clearances and preloads.

PARAMETER	*50% OFFSET*	*60% OFFSET*
Radial Bearing Clearance, C_b	.0814 mm (.0032 in)	.0837 mm (.0033 in)
Measured Preload, M_p	0.27	0.25

EXPERIMENTAL PROCEDURE

The testing procedure achieves steady-state conditions and data acquisition. Test conditions include four running speeds varying from 7 to 16 krpm and six static unit loads from 0 to 3101 kPa (450 psi). The oil flow-rate is constant for each running speed. Table 3 presents a matrix of the nominal test conditions for unit load, rotor speed, and oil flow-rate. The inlet oil inlet temperature was maintained at 43.3°C (110°F).

Table 3. Matrix of nominal test conditions.

Static Load kPa (*psi*)	**Speed [RPM],** *Flow-rate [gpm]* **7000**, *5.5*	**10000**, *5.5*	**13000**, *8.0*	**16000**, *10*
0 (*0*)	✓	✓	✓	✓
345 (*50*)	✓	✓	✓	✓
1034 (*150*)	✓	✓	✓	✓
1723 (*250*)	✓	✓	✓	✓
2413 (*350*)	✓	✓	✓	✓
3101 (*450*)	✓	✓	✓	✓

Dynamic Stiffness-Coefficients

Rotordynamic coefficients are extracted from the measured dynamic data via the parameter identification approach described by Childs and Hale [15] and Rouvas and Childs [16]. To start, the equation of motion for the stator mass M_s can be written by applying Newtons's Second Law in the *x* and *y* directions, as shown below.

$$M_s\begin{bmatrix}\ddot{x}_s\\ \ddot{y}_s\end{bmatrix}=\begin{bmatrix}f_x\\ f_y\end{bmatrix}-\begin{bmatrix}f_{bx}\\ f_{by}\end{bmatrix} \tag{3}$$

In Eq.(3), $\ddot{x}_s$ and $\ddot{y}_s$ are the absolute stator accelerations, f_x and f_y are the excitation forces, and f_{bx} and f_{by} are the bearing reaction forces. Substituting the [K][C][M] bearing reaction force model from Eq. (2) and rearranging yields

$$\begin{bmatrix}f_x-M_s\ddot{x}_s\\ f_y-M_s\ddot{y}_s\end{bmatrix}=-\begin{bmatrix}K_{xx} & K_{xy}\\ K_{yx} & K_{yy}\end{bmatrix}\begin{bmatrix}\Delta x\\ \Delta y\end{bmatrix}-\begin{bmatrix}C_{xx} & C_{xy}\\ C_{yx} & C_{yy}\end{bmatrix}\begin{bmatrix}\Delta\dot{x}\\ \Delta\dot{y}\end{bmatrix}-\begin{bmatrix}M_{xx} & M_{xy}\\ M_{yx} & M_{yy}\end{bmatrix}\begin{bmatrix}\Delta\ddot{x}\\ \Delta\ddot{y}\end{bmatrix} \tag{4}$$

The left side terms as well as the Δx and Δy terms are measured directly. Extracting rotordynamic coefficients occurs in the frequency domain and requires performing an FFT, yielding

$$\begin{bmatrix}\boldsymbol{F}_x-M_s\boldsymbol{A}_x\\ \boldsymbol{F}_y-M_s\boldsymbol{A}_y\end{bmatrix}=-\begin{bmatrix}\boldsymbol{H}_{xx} & \boldsymbol{H}_{xy}\\ \boldsymbol{H}_{yx} & \boldsymbol{H}_{yy}\end{bmatrix}\begin{bmatrix}\boldsymbol{D}_x\\ \boldsymbol{D}_y\end{bmatrix} \tag{5}$$

The parameters $\boldsymbol{F}$, $\boldsymbol{A}$, and $\boldsymbol{D}$ are the Fourier transforms of the excitation force, absolute stator acceleration, and the relative stator to rotor motion for the *x* and *y* directions. $\boldsymbol{H_{ij}}$ is the complex dynamic stiffness that relates a force in the "*i*" direction in response to a motion in the "*j*" direction. In terms of the rotordynamic coefficients, the $\boldsymbol{H_{ij}}$ coefficients are written,

$$\boldsymbol{H}_{ij}=K_{ij}-\Omega^2M_{ij}+\boldsymbol{j}(\Omega C_{ij}) \tag{6}$$

Taking the real and imaginary components of the dynamic stiffness yields:

$$\mathrm{Re}(\boldsymbol{H}_{ij})=K_{ij}-\Omega^2M_{ij} \tag{7}$$

$$\mathrm{Im}(\boldsymbol{H}_{ij})=\Omega C_{ij} \tag{8}$$

Where Ω is the excitation frequency. Equation (7) shows that the stiffness and added mass coefficients can be estimated by curve fitting the Re($\boldsymbol{H_{ij}}$) with a quadratic function of Ω. Estimates for the damping coefficients are obtained from the slope of the Im($\boldsymbol{H_{ij}}$) with respect to Ω as shown in Eq. (8).

Equation (5) provides two equations for the four unknowns $\boldsymbol{H_{xx}}$, $\boldsymbol{H_{xy}}$, $\boldsymbol{H_{yx}}$, and $\boldsymbol{H_{yy}}$. Four equations are obtained by shaking the stator in the *x* and *y* directions while measuring the response in both directions to obtain

$$\begin{bmatrix}\boldsymbol{F}_{xx}-M_s\boldsymbol{A}_{xx} & \boldsymbol{F}_{xy}-M_s\boldsymbol{A}_{xy}\\ \boldsymbol{F}_{yx}-M_s\boldsymbol{A}_{yx} & \boldsymbol{F}_{yy}-M_s\boldsymbol{A}_{yy}\end{bmatrix}=-\begin{bmatrix}\boldsymbol{H}_{xx} & \boldsymbol{H}_{xy}\\ \boldsymbol{H}_{yx} & \boldsymbol{H}_{yy}\end{bmatrix}\begin{bmatrix}\boldsymbol{D}_{xx} & \boldsymbol{D}_{xy}\\ \boldsymbol{D}_{yx} & \boldsymbol{D}_{yy}\end{bmatrix} \tag{9}$$

Frequency-dependent $\boldsymbol{H_{ij}}$ coefficients are obtained for a single shake from 32 repeated excitations that are averaged in the frequency domain. Excitations use a pseudo-random waveform that includes frequencies from 20 to 320 Hz in approximately 10 Hz increments. For each experimental condition, 10 consecutive shakes are conducted in the *x* and *y* directions, providing 320 waveforms applied in each direction at each steady state test condition.

To account for the stiffness and damping of all the stator attachments, a *baseline* or dry dynamic test is performed at zero speed before any lubricating oil enters the bearing, measuring the dynamic stiffness of the stator attachments without the effect of fluid inertia or dynamics. Subtracting the baseline results from the dynamic stiffness measured during testing yields the dynamic stiffness of the fluid film only.

RESULTS

Dynamic Stiffness Coefficients

Dynamic stiffness coefficients were obtained for all steady-state test conditions provided in Table 3. The results presented are for the test bearing only, meaning the baseline has already been subtracted. Fig. 5 presents the measured $\boldsymbol{H}_{ij}$ coefficients and curve fits used to determine rotordynamic coefficients for 50 and 60% offsets at the highest speed and zero unit load condition. Note: The uncertainty bars represent the repeatability of the dynamic stiffness values from the 10 shake tests.

Fig. 5 (a) compares the direct real dynamic stiffness functions and shows that the 60% offset bearing is considerably stiffer in both orthogonal directions. In addition, the 60% offset direct real $\boldsymbol{H}_{xx}$ and $\boldsymbol{H}_{yy}$ curves have an upward curvature with increasing Ω while the 50% offset values are less variable with changing Ω, demonstrating that the M_{xx} and M_{yy} coefficients will be negative and larger in magnitude for the 60% offset.

The Im($\boldsymbol{H}_{xx}$) and Im($\boldsymbol{H}_{yy}$) coefficients shown in Fig. 5 (b) are almost the same for the 50 and 60% offset, meaning C_{xx} and C_{yy} are almost identical for both offsets. For both offsets, the Im($\boldsymbol{H}_{xx}$) and Im($\boldsymbol{H}_{yy}$) increase linearly with increasing Ω, allowing for frequency independent direct damping coefficients.

Re($\boldsymbol{H}_{xy}$) and Re($\boldsymbol{H}_{yx}$) are plotted in Fig. 5 (c). The zero frequency intercepts for Re($\boldsymbol{H}_{xy}$) and Re($\boldsymbol{H}_{yx}$) are larger for the 60% offset, showing that the 60% offset will have larger cross-coupled stiffness coefficients. For both offsets, the Re($\boldsymbol{H}_{yx}$) decreases with increasing Ω while the Re($\boldsymbol{H}_{xy}$) increases with increasing Ω. This opposing curvature gives M_{xy} and M_{yx} of opposite signs, implying a negative impact on stability.

In Fig. 5 (d), Im($\boldsymbol{H}_{xy}$) and Im($\boldsymbol{H}_{yx}$) show a linear dependence with Ω for both pivot offsets. They have larger slopes for the 60% offset, meaning C_{xy} and C_{yx} are larger for the 60% offset. For both pivot offsets, C_{xy} and C_{yx} have the same sign, indicating true dissipation versus gyroscopic damping.

Table 4 gives the numerical values and uncertainties of the rotordynamic coefficients at the 16 krpm and zero unit load. These uncertainty values represent the quality of the curve fit through the average dynamic stiffness coefficients.

Table 4. Rotordynamic coefficients at 16 krpm and zero load.

COEFFICIENT	UNITS	50% OFFSET		60% OFFSET	
		value	uncert.	value	uncert.
K_{xx}	[MN/m]	255.0	6.6	276.6	20.1
K_{yy}	[MN/m]	295.1	6.8	325.3	2.1
C_{xx}	[kN-s/m]	153.3	7.6	170.3	31.8
C_{yy}	[kN-s/m]	178.4	9.8	178.3	7.3
M_{xx}	[kg]	-2.7	7.5	-23.2	27.4
M_{yy}	[kg]	11.3	7.7	-11.9	2.9
K_{xy}	[MN/m]	-1.4	2.5	8.4	4.4
K_{yx}	[MN/m]	72.9	7.5	93.4	12.2
C_{xy}	[kN-s/m]	45.0	3.5	59.9	4.9
C_{yx}	[kN-s/m]	6.4	11.7	35.1	28.2
M_{xy}	[kg]	-1.0	2.9	-6.8	6.0
M_{yx}	[kg]	15.4	8.5	17.1	16.6

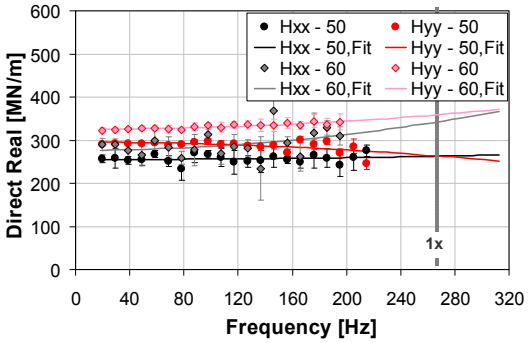

(a) direct real

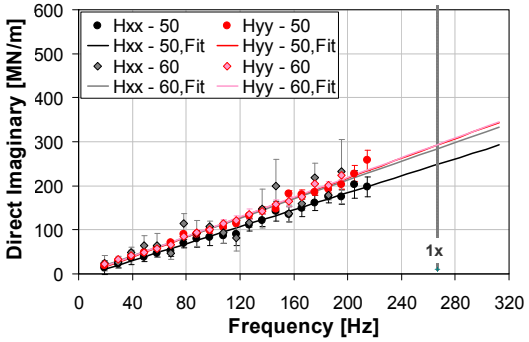

(b) direct imaginary

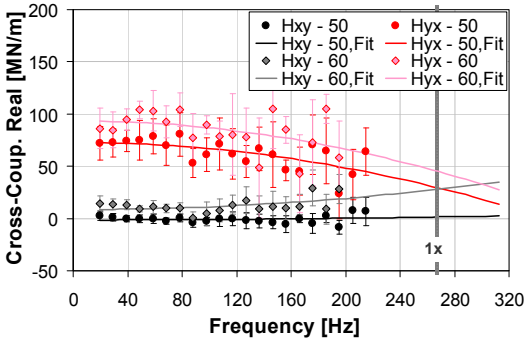

(c) cross-coupled real

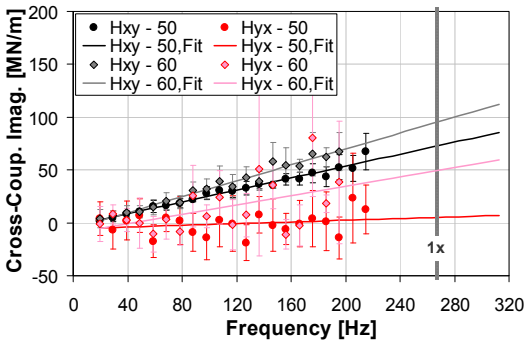

(d) cross-coupled imaginary

Fig. 5. 50 and 60% offset measured dynamic stiffness at 16 krpm and zero unit load for: (a) direct real, (b) direct imaginary, (c) cross-coupled real, (d) cross-coupled imaginary.

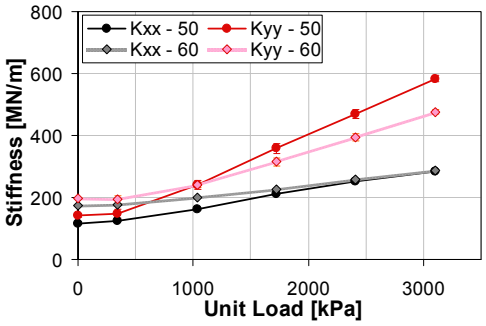

(a) 7 krpm

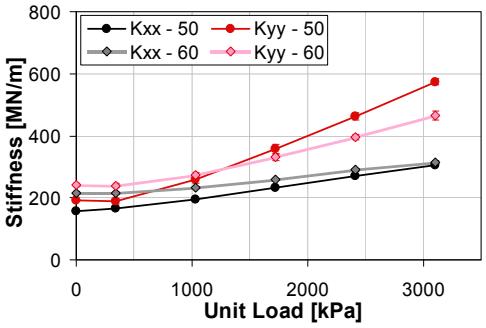

(b) 10 krpm

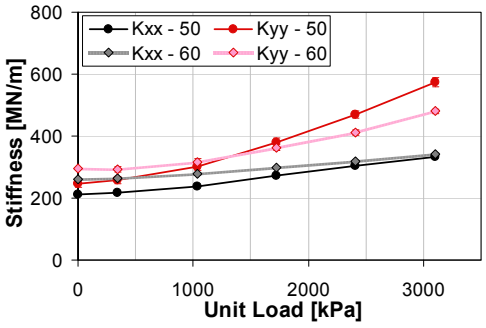

(c) 13 krpm

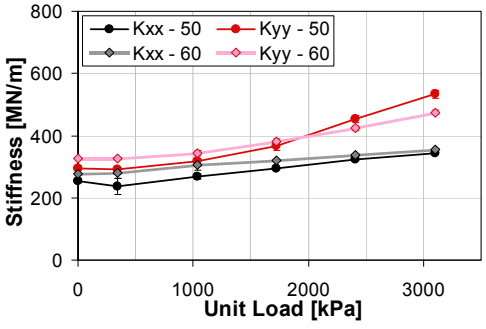

(d) 16 krpm

Fig. 6. Direct stiffness coefficients at (a) 7 krpm, (b) 10 krpm, (c) 13 krpm, (d) 16 krpm.

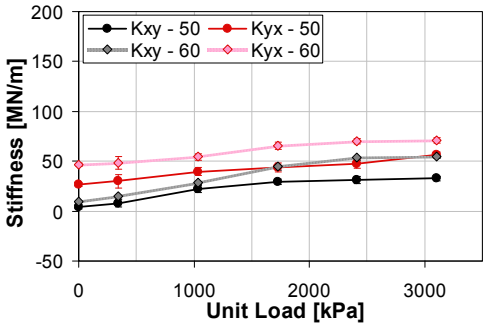

(a) 7 krpm

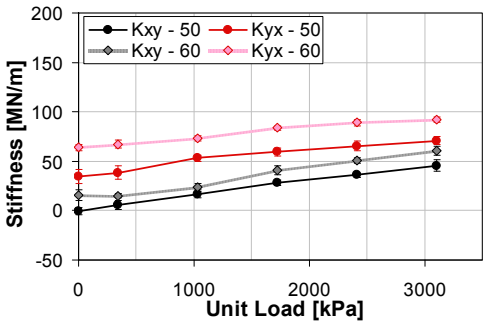

(b) 10 krpm

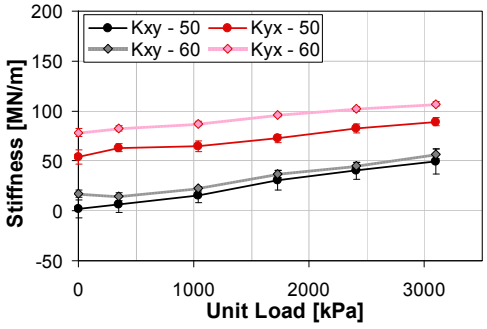

(c) 13 krpm

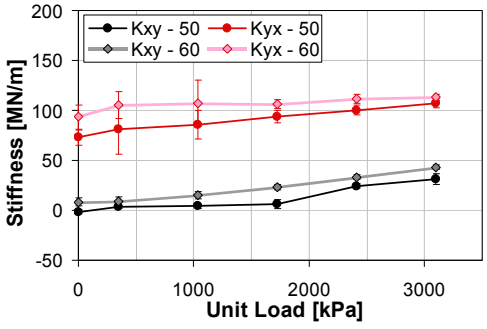

(d) 16 krpm

Fig. 7. Cross-coupled stiffness coefficients at (a) 7 krpm, (b) 10 krpm, (c) 13 krpm, (d) 16 krpm.

Stiffness Coefficients

K_{xx} and K_{yy} coefficients are plotted with respect to unit load in Fig. 6. At light unit loads, K_{yy} for the 60% offset is measurably higher than for the 50% offset. This chacteristic in K_{yy} reverses with increasing unit load where the 50% offset K_{yy} is larger than the 60% offset. K_{xx} is larger for the 60% offset at light loads, and both offsets approach the same K_{xx} value with increasing load.

Fig. 7 presents K_{xy} and K_{yx} coefficients versus unit load, showing that they are slightly larger for the 60% offset than the 50% offset. For both offsets, K_{yx} is always larger than K_{xy}, and both have the same sign.

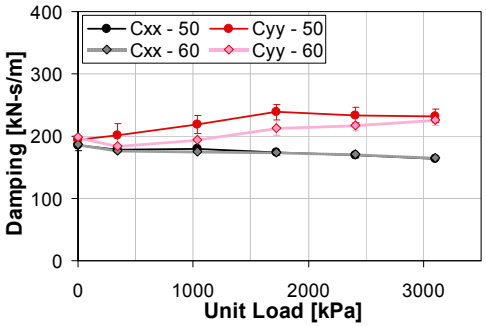

(a) 7 krpm

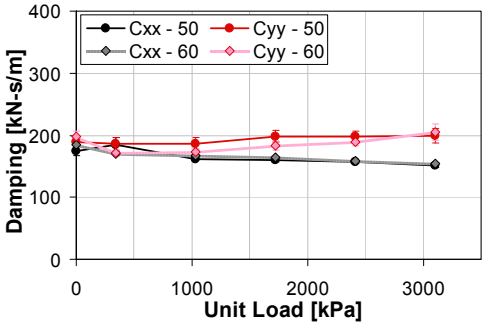

(b) 10 krpm

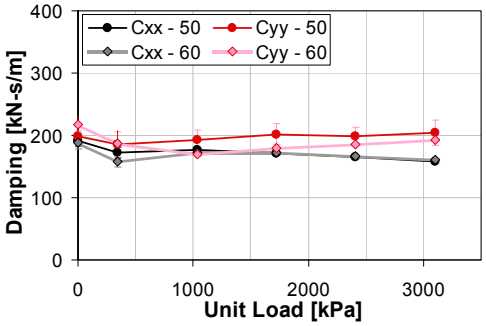

(c) 13 krpm

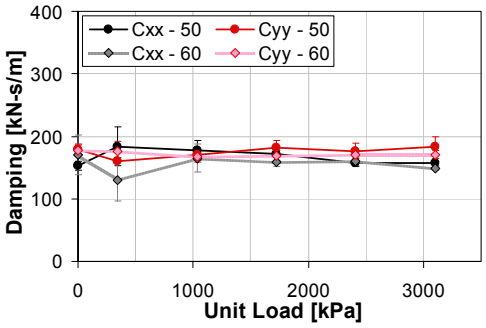

(d) 16 krpm

Fig. 8. Direct damping coefficients at (a) 7 krpm, (b) 10 krpm, (c) 13 krpm, (d) 16 krpm.

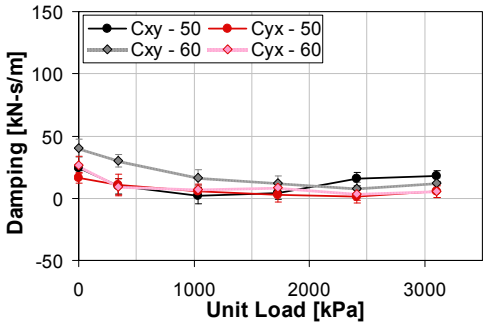

(a) 7 krpm

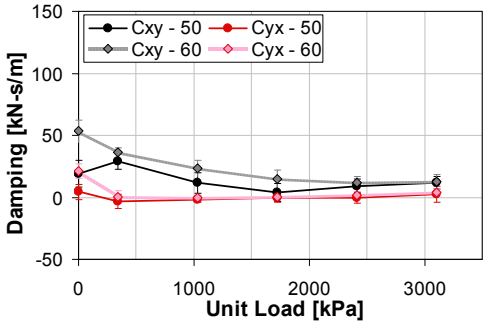

(b) 10 krpm

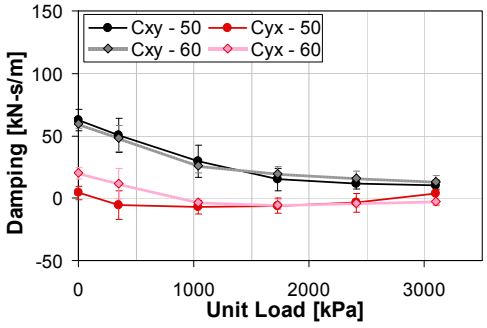

(c) 13 krpm

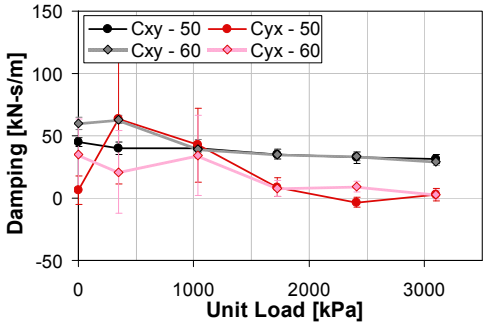

(d) 16 krpm

Fig. 9. Cross-coupled damping coefficients at (a) 7 krpm, (b) 10 krpm, (c) 13 krpm, (d) 16 krpm.

Damping Coefficients

C_{yy} and C_{xx} coefficients are plotted with respect to unit load for four rotor speeds in Fig. 8. No appreciable difference arises in direct damping between 50 and 60% offsets for most test conditions. Regardless of offset, the direct damping coefficients show slight dependency on unit load or ω.

Fig. 9 presents the C_{xy} and C_{yx} coefficients. As with the direct coefficients, they do not show a significant difference between pivot offsets. Both offsets show C_{xy} to be usually larger than C_{yx} for the higher test speeds. Additionally, C_{yx} is consistently near zero for most speeds and loads.

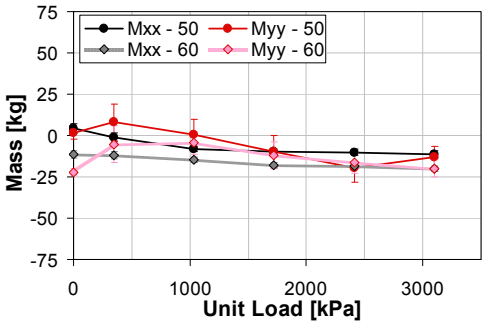

(a) 7 krpm

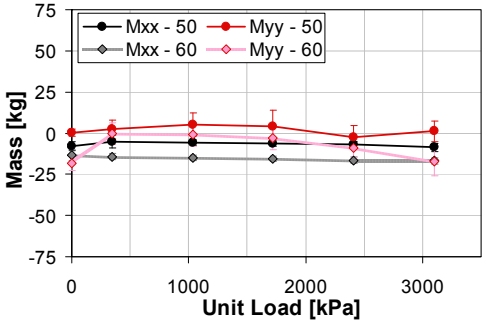

(b) 10 krpm

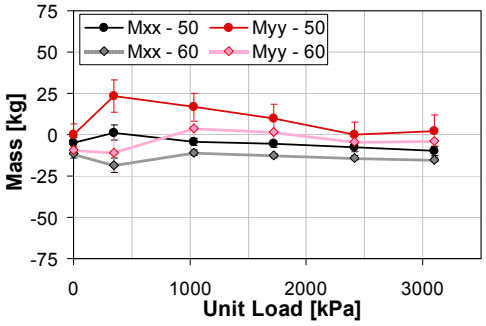

(c) 13 krpm

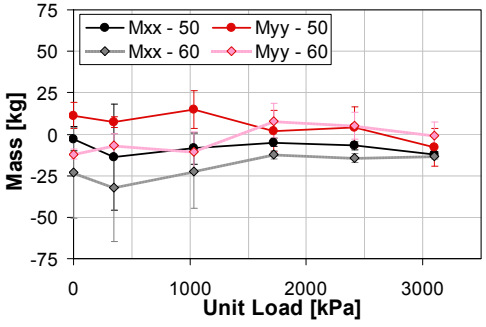

(d) 16 krpm

Fig. 10. Direct added-mass coefficients at (a) 7 krpm, (b) 10 krpm, (c) 13 krpm, (d) 16 krpm.

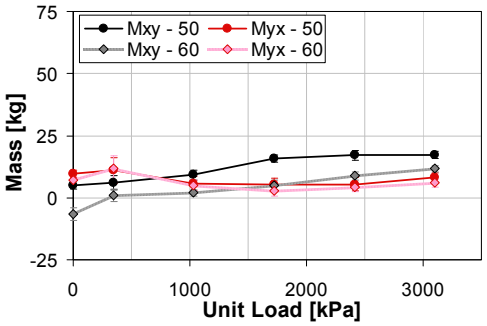

(a) 7 krpm

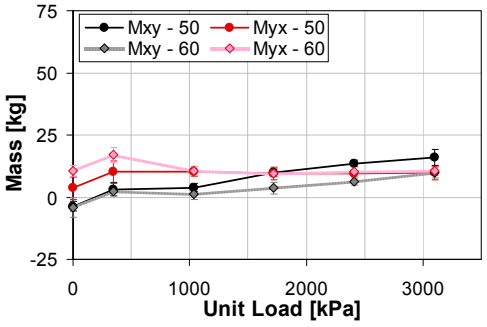

(b) 10 krpm

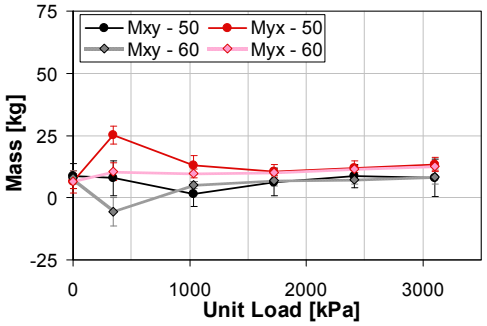

(c) 13 krpm

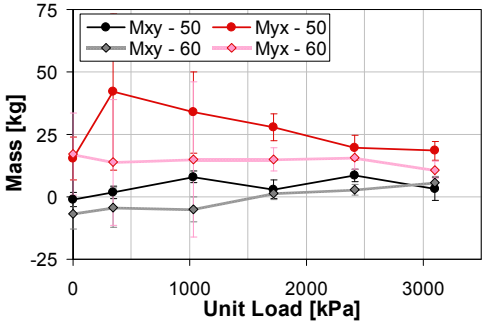

(d) 16 krpm

Fig. 11. Cross-coupled added-mass coefficients at (a) 7 krpm, (b) 10 krpm, (c) 13 krpm, (d) 16 krpm.

Added-Mass Coefficients

The M_{xx} and M_{yy} coefficients are presented in Fig. 10 for both pivot offsets. M_{xx} and M_{yy} are slightly more positive (less negative) for the 50% offset than for the 60% configuration. M_{yy} is more positive than M_{xx} for both offsets. The largest positive added-mass coefficients are usually the 60% offset M_{yy} while the most negative added-mass term is typically M_{xx} of the 50% offset.

Fig. 11 shows the M_{xy} and M_{yx} coefficients versus static unit load. M_{xy} and M_{yx} are comparable for both pivot offsets. Over most test conditions, M_{xy} and M_{yx} are positive and are typically less than 25 kg for both the 50 and 60% offset. Additionally, M_{xy} and M_{yx} usually have the same sign, showing no impact on stability.

Static Data

Static eccentricity measurements were taken at each steady-state test condition. Figure 12 provides the eccentricity plots for the 50 and 60% offsets. The eccentricities presented are normalized with respect to the bearing clearance. Each data point represents a static load condition, with the centered position representing the zero load condition. Minimal cross-coupling exists for either offset. The attitude angle measured from the loaded axis increases with increasing ω, with a maximum of about 10° at 16 krpm. No appreciable difference in eccentricity is measured between pivot offsets.

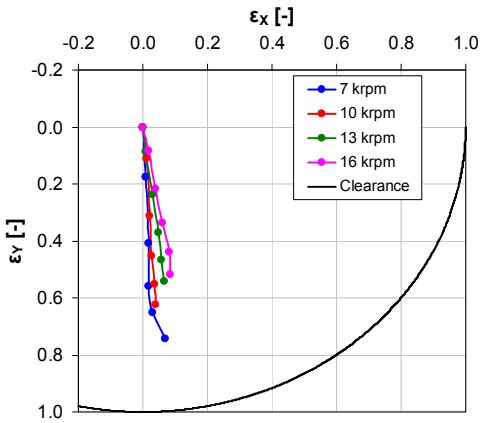

(a) 50% offset

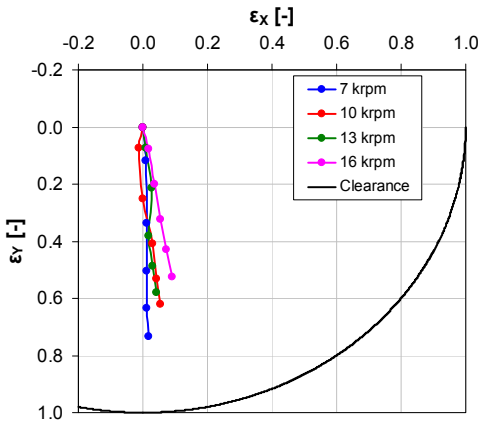

(b) 60% offset

Fig. 12. Dynamic and static stiffness in the loaded direction for (a) 50% offset, (b) 60% offset.

Fig. 13 presents the dynamically-predicted stiffness *Kyy* (*y* is the direction of the static load) and static stiffness K_s for the loaded direction for ω = 16 krpm. K_s is estimated as the derivative from the static load versus displacement curve. K_s offers a benchmark to compare K_{yy} that was estimated from the multi-frequency testing. Agreement between K_{yy} and K_s is within 20% for all cases, with K_s consistenly larger than K_{yy}. Different factors can contribute to the discrepancies between K_{yy} and K_s, including the thermal distortion of the bearing stator and rotor. During testing, the stator assembly and the shaft may experience some expansion because of the elevated temperatures, thus impacting the steady state displacement and therefore K_s. While thermal effects can impact motion measurements between test conditions, these effects have a minimal effect on the relative motion measurements that are taken during each steady-state condition, i.e., during testing for dynamic-stiffness coefficients. Hence, K_{yy} may be the more accurate measurement of the direct stiffness coefficient for the loaded direction.

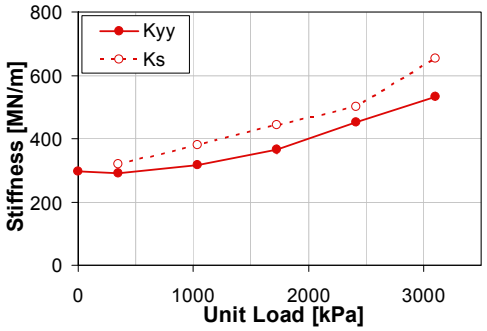

(a) 50% offset

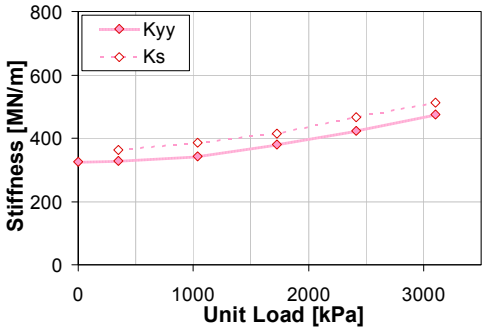

(b) 60% offset

Fig. 13. Dynamic and static stiffness at 16 krpm in the loaded direction for (a) 50% offset, (b) 60% offset.

SUMMARY, DISCUSSION, AND CONCLUSION

Rotordynamic coefficients including stiffness, damping, and added-mass coefficients were determined from measured complex dynamic stiffnesses. For 50 and 60% offsets, the direct and cross-coupled real parts of the dynamic stiffness exhibited frequency dependency that could be accounted for (simply) with added-mass coefficients, resulting in frequency-independent stiffness and added-mass coefficients. The imaginary parts of the measured dynamic stiffness increased linearly with increasing excitation frequency Ω for both offsets, allowing for frequency-independent damping coefficients.

For many test conditions, the direct dynamic stiffnesses showed an increase with increasing frequency that could be modeled with negative added-mass coefficients. This "hardening" effect is indicative of a spring in series with spring-damper combination as shown below in Fig. 14.

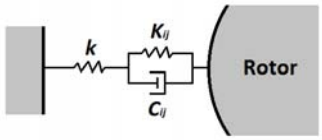

Fig. 14. Spring in series with a fluid film model.

Here, the damper-spring combination represents the fluid film stiffness and damping while the single spring represents the pivot-support stiffness of the bearing. This system can be described in terms of an equivalent stiffness and damping coefficients. The Taylor expansion of the equivalent stiffness indicates that stiffness will increase with increasing excitation frequency. The measured Re($\boldsymbol{H}_{xx}$) and Re($\boldsymbol{H}_{yy}$) of the test bearings often followed this trend,

suggesting that pivot stiffness could be important. Additionally, the expansion of equivalent damping shows a damping decrease or fall off with increasing frequency. However, the experimental damping from the test bearings did not indicate any frequency dependency.

Stiffness orthotropy existed for each pivot offset at zero unit loads. At low static loads, the direct stiffness coefficients were larger for the 60% offset configuration than for the 50% offset. For large loads, K_{xx} was about the same for each offset while K_{yy} was larger for the 50% offset. Cross-coupled stiffness coefficients were positive and considerably smaller than the direct stiffness coefficients for both offsets.

The direct damping coefficients generally did not vary with respect to changes in unit load and showed only a slight dependency with respect to changes in ω. Cross-coupled damping coefficients were considerably smaller than the direct damping. C_{xy} and C_{yx} were positive for both pivot offsets, implying real and positive damping. Direct and cross-coupled damping coefficients did not show an appreciable change with respect to the tested pivot offsets.

Added-mass coefficients for both offsets were able to capture the frequency dependency of the measured dynamic stiffness at all test conditions. For both pivot offsets, M_{xx} was consistently negative and M_{yy} was usually more positive. Comparing offsets, both direct added-mass coefficients were more positive (less negative) for the 50% offset. The cross-coupled added-mass coefficients were generally positive for both pivot offsets. M_{xy} and M_{yx} generally had the same sign for both offsets, indicating no impact on stability. The largest added-mass magnitudes approached 32 kg (70 lb).

The 60% offset bearing tested here is almost identical to that tested by Carter and Childs [8]. However, the dynamic stiffnesses and rotordynamic coefficients showed differences from [8] that are credited to a changed motion-probe location used for the current testing. The probes locations were changed from a position that was on the opposite side of the bearing from the stinger connection to the same side to minimize the effect of stator flexibility. This flexibility effects the displacement measurements that are used in determining dynamic stiffness coefficients, thus impacting the rotordynamic coefficients. The current probe setup is believed to be more accurate than the orientation used by Carter and Childs [8] because it places the motion probe near the load path of the dynamic force. More details are provided by Kulhanek [12]. The direct stiffness and damping coefficients presented here are ~10 to 25% lower than those presented in [8]. The new probe setup also produced M_{xx} and M_{yy} values that were sometimes negative and generally smaller in magnitude. K_{xy} and K_{yx} obtained here were typically both positive while in [8], K_{xy} and K_{yx} values had opposite signs. Additionally, the current test setup allows for meaningful estimates for C_{xy} and C_{yx}.

Overall, the dynamic stiffnesses and rotordynamic coefficient trends in this work agree with the test results of Delgado et al. [11]. At light unit loading, the direct stiffness coefficients were considerably larger for the 60% offset than the 50% offset, comparable to Delgado et al. Additionally, Delgado et al. did not observe an appreciable difference in direct damping for different pivot offsets, similar to the direct damping presented in this thesis. Delgado et al. obtained positive and negative direct added-mass coefficients with the largest magnitude approaching 23 kg, comparable to the values cited here.

REFERENCES

[1] Lund, J.W., 1964, "Spring and Damping Coefficients for the Tilting-Pad Journal Bearing," ASLE Trans., **7**, pp. 342-352.

[2] Ha, H., and Yang, S., 1999, "Excitation Frequency Effects on the Stiffness and Damping Coefficients of a Five-Pad Tilting Pad Journal Bearing," ASME J. Tribol., **121**, pp. 517-522.

[3] Wygant, K. D., 2001 "The Influence of Negative Preload and Nonsynchronous Excitation on the Performance of Tilting Pad Journal Bearings," Ph.D. Dissertation, Univ. of Virginia, Charlottesville, Virginia.

[4] Rodriguez, L., and Childs, D., 2006, "Frequency Dependency of Measured and Predicted Rotordynamic Coefficients for Load-on-Pad Flexible-Pivot Tilting-Pad Bearing," ASME J. Tribol., **128** (2), pp. 388-395.

[5] Al-Ghasem, A., and Childs, D., 2006, "Measurements Versus Predictions for a High-Speed Flexure-Pivot Tilting-Pad Bearing (Load-Between-Pad Configuration)," ASME J. Eng. Gas Turbines Power, **128** (4), pp. 896-906.

[6] Hensley, E. J., and Childs, D., 2008, "Measurements versus Predictions for the Rotordynamic Characteristics of a Flexure Pivot-Pad Tilting Pad Bearing in an LBP Condition at Higher Unit Loads," Proceedings of ASME Turbo Expo 2008, Paper GT2008-50069, June 9-13, Berlin, Germany.

[7] Dmochowski, W., 2006, "Dynamic Properties of Tilting-Pad Journal Bearings: Experimental and Theoretical Investigation of Frequency Effects Due to Pivot Flexibility," ASME Turbo Expo 2006: Power for Land, Sea and Air Barcelona, Spain.

[8] Carter, C., and Childs, D., 2008 "Measurements versus Predictions for the Rotordynamic Characteristics of a 5-Pad, Rocker-Pivot, Tilting-Pad Bearing in Load Between Pad Configuration," Proceedings of ASME Turbo Expo 2008, Paper GT2008-50069, June 9-13, Berlin, Germany.

[9] Childs, D., and Harris, J., 2009, "Static Performance Characteristics and Rotordynamic Coefficients for a Four-Pad Ball-in-Socket Tilting Pad Journal Bearing," ASME J. Eng. Gas Turbines Power, **131**, 062502.

[10] Schmeid, J., Fedorov, A., and Grigoriev, B., 2010, "Non-Synchronous Tilting Pad Bearing Characteristics," Proceedings of the 10th IFToMM International Conference on Rotordynamics, September 12-15, Seoul, Korea.

[11] Delgado, A., Ertas, B., Drexel M., Naldi, L., and Vannini, G., 2010, "Identification and Prediction of Force Coefficients in a Five-Pad and Four-Pad Tilting Pad Bearing for Load-on-Pad and Load-Between-Pad Configurations," Proceedings of ASME Turbo Expo 2010, Paper GT2010-23802, June 14-18, Glasgow, UK.

[12] Kulhanek, C., 2010, "Dynamic and Static Characteristics of a Rocker-Pivot, Tilting-Pad Bearing with 50% and 60% Offsets," M.S. thesis, Mechanical Engineering, Texas A&M University, College Station, TX.

[13] Kaul, A., 1999, "Design and Development of a Test Setup for the Experimental Determination of the Rotordynamic and Leakage Characteristics of Annular Bushing Oil Seals," M.S. thesis, Mechanical Engineering, Texas A&M University, College Station, TX.

[14] Glienicke, J., 1966, "Experimental Investigation of Stiffness and Damping Coefficients of Turbine Bearings and Their Application to Instability Predictions," Proceedings of the International Mech. E., **181** (3B), pp. 116-129. a

[15] Childs, D., and Hale, K., 1994, "A Test Apparatus and Facility to Identify the Rotordynamic Coefficients of High-Speed Hydrostatic Bearings," ASME J. of Trib., **116**, pp. 337-344.

[16] Rouvas, C., and Childs, D., 1993, "A parameter Identification Method for the Rotordynamic Coefficients of a High Reynolds Number Hydrostatic Bearing," ASME J. of Vibration and Acoustics, **115**, pp. 264-270.